

BTSeg: Barlow Twins Regularization for Domain Adaptation in Semantic Segmentation

Johannes Künzel Anna Hilsmann Peter Eisert

Fraunhofer Heinrich-Hertz-Institute, Berlin – Humboldt University Berlin, Berlin

{johannes.kuenzel, anna.hilsmann}@hhi.fraunhofer.de

peter.eisert@hu-berlin.de

Abstract

Semantic image segmentation is particularly vital for the advancement of autonomous vehicle technologies. However, this domain faces substantial challenges under adverse conditions like rain or darkness, which remain under-represented in most datasets. The generation of additional training data for these scenarios is not only costly but also fraught with potential inaccuracies, largely attributable to the aleatoric uncertainty inherent in such conditions.

We introduce BTSeg, an innovative, semi-supervised training approach enhancing semantic segmentation models in order to effectively handle a range of adverse conditions without requiring the creation of extensive new datasets. BTSeg employs a novel application of the Barlow Twins loss, a concept borrowed from unsupervised learning. The original Barlow Twins approach uses stochastic augmentations in order to learn useful representations from unlabeled data without the need for external labels. In our approach, we regard images captured at identical locations but under varying adverse conditions as manifold representation of the same scene (which could be interpreted as "natural augmentations"), thereby enabling the model to conceptualize its understanding of the environment.

We evaluate our approach on the ACDC dataset, where it performs favorably when compared to the current state-of-the-art methods, while also being simpler to implement and train. For the new challenging ACG benchmark it shows cutting-edge performance, demonstrating its robustness and generalization capabilities. We will make the code publicly available post-acceptance.

1. Introduction

In autonomous driving, semantic segmentation encounters heightened challenges in adverse conditions, including snow, rain, fog, and darkness. Precisely annotating images pixel-by-pixel under such conditions is costly and difficult;

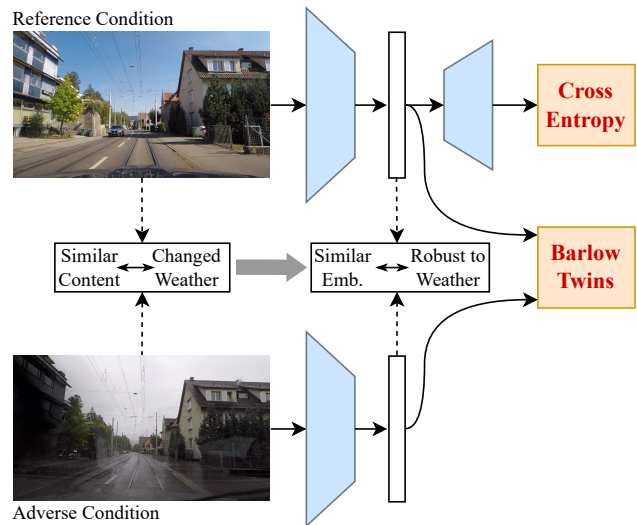


Figure 1. BTSeg employs the Barlow Twins loss as regularization in a semantic segmentation network, processing two images captured at the same location under different weather conditions. These images, viewed as augmented versions of a base image by the Barlow Twins approach, enable the network to generate encodings that not only accurately estimate semantic segmentation but also withstand appearance variations due to changing weather, through the combined use of Barlow Twins loss and Cross Entropy loss.

consider, for example, the challenge of distinguishing between a road and a sidewalk in snowy conditions. Recent datasets introduced by [23] and [22] contain pairs of images, taken under adverse and clear weather respectively, roughly aligned using their respective GPS coordinates.

Taking advantage of these datasets, we present BTSeg (Barlow Twins [30] regularized Segmentation), a novel semi-supervised training strategy for learning semantic segmentation models, which are robust to varying weather conditions, visualized in Fig. 1.

The Barlow Twins methodology trains an encoder us-

ing two different augmentations of the same image, aiming for feature consistency despite the augmentations (see Sec. 3.1 for a brief introduction). Opposed to that, BTSEg treats the roughly matched image pairs depicting differing weather conditions as natural augmentations. These pairs are leveraged to teach the network’s encoder to find and use the latent information shared by both scenarios.

We argue that generating high-quality ground truth data is easier for clear weather images. Thus, BTSEg incorporates their annotations into a second objective function to compel the encoder to produce feature maps suitable for generating high-quality segmentations.

In summary, our main contributions are the following:

- We introduce the integration of the Barlow Twins framework into semantic segmentation for increased robustness under adverse conditions in a semi-supervised manner. This eliminates the need for elaborately annotated bad weather conditions or negative samples as in earlier contrastive methods, such as [4].
- We provide effective solutions for challenges inherent to image pairs taken under realistic conditions, such as moving objects and slightly misaligned images,
- We demonstrate how our approach can easily be integrated in common semantic segmentation networks, consisting of an encoder and a decoder part, while introducing only a negligibly increase in the number of parameters.
- Our approach shows favorable results when compared against current state-of-the-art methods, setting a new state-of-the-art for the challenging ACG-benchmark, indicating both its efficiency and effectiveness.

The rest of this paper includes a review of related work (Sec. 2), an introduction to Barlow Twins (Sec. 3.1), and our approach for integrating it with semantic segmentation (Sec. 3.2). We discuss addressing alignment challenges in training data (Sec. 3.4–Sec. 3.5) from GPS-matched image pairs. In Sec. 4, our approach is thoroughly evaluated against current state-of-the-art methods, examining design choices and assessing generalization and robustness. We conclude with a summary, limitations, and future research directions in Sec. 5.

2. Related work

In this section, we briefly review the state-of-the-art in image segmentation under adverse conditions, self-supervised learning and combination thereof.

2.1. Weakly-supervised domain adaption

With the introduction of datasets like Dark Zurich [22] and ACDC [23], the field of semantic image segmentation has expanded to include adverse weather conditions. These datasets consist of images captured under different lighting

situations and adverse conditions, each with manually created semantic segmentation paired with a reference image taken under favorable weather conditions. This has paved the way for weakly-supervised domain adaptation methods that leverage the information in this association.

Sakaridis *et al.* [24] gradually adapt from the daytime to the nighttime domain using images from different lighting situations. They extract information from the reference-to-target image pairing and use artificially stylized annotated images. Bruggemann *et al.* [5] introduced an uncertainty-aware ALIGN-module to improve the alignment between reference and target domains, omitting the usage of stylized images and the gradual adaptation procedure.

In another work by Bruggemann *et al.* [4], a contrastive loss formulation in the embedding space is used to learn weather-condition-robust features. This procedure requires maintaining a list of negative samples for each positive sample, which can complicate implementation and impede training if the negatives are too close to the positives.

2.2. Self-supervised learning

Self-supervised learning methods have been developed to leverage the intrinsic structure of unlabeled data. These methods typically generate synthetic augmentations of input images, training networks to produce feature representations that are invariant to such changes. However, without careful design, networks may collapse to a trivial solution where they output constant features that do not depend on the data.

To mitigate this, contrastive-based methods, such as those by Chen *et al.* [8] and Misra *et al.* [18], have been introduced. These methods enforce a closer similarity between features of augmented images from the same source (positive pairs) than those from different sources (negative pairs). The selection of negative samples is crucial in these approaches to prevent the network from settling into degenerate solutions.

Clustering-based approaches [1, 6], group images into clusters, aiming to ignore any augmentations. These methods must carefully manage the clustering process to avoid all embeddings converging into a single cluster, another form of the trivial solution.

The Barlow Twins method, introduced by Zbontar *et al.* [30], employs redundancy reduction techniques, notably avoiding the use of negative pairs, asymmetric updates, stopped gradients, or non-differentiable operators. It circumvents the trivial solution through a loss function that encourages the cross-correlation matrix of batch-normalized embeddings of augmented image pairs to approximate the identity matrix.

Building on this, Bardes *et al.* [2] presented VICReg, which incorporates two separate regularization terms applied to each embedding and a third term to ensure the em-

beddings remain similar. This model introduces additional hyperparameters due to the need to balance these terms. However, since VICReg did not demonstrate significant improvements over the Barlow Twins’ approach, we have chosen to employ the latter in our method.

2.3. Barlow Twins for semantic segmentation

The Barlow Twins methodology has been adopted in the segmentation of medical imagery with notable success, as reported by Siddiquee *et al.* [25] and Punn *et al.* [19]. Unlike our approach, these methods rely on traditional augmentation strategies, as described in the seminal work by Zbontar *et al.* [30].

The work of Bhagwatkar *et al.* in [3] exploits the Barlow Twins loss formulation [30] to train an encoder network robust against “domain transformations” and assumes “corresponding images from different domains as different views of the same abstract representation”. Additionally, they jointly train a segmentation head for one domain, utilizing the output of the encoder. However, they try to adapt from synthetic to real data, but it remains unclear how to select corresponding images in this setting. As a result, unlike our method, the images they use lack closely related semantic content. We posit that this could hinder the encoder training, as it must reconcile the creation of similar embeddings for dissimilar image contents. While this may enhance robustness to domain shifts, it simultaneously compels the encoder to reconcile divergent image contents, presenting conflicting training goals.

In contrast, our work utilizes natural, paired images of identical locales captured in both clear and adverse environmental conditions. Furthermore, we implement sophisticated techniques to manage dynamic content and reconcile misaligned perspectives, thus addressing issues beyond those tackled by previous methods.

3. Method

This section outlines our methodology, which exploits the Barlow Twins loss to fortify semantic segmentation networks against domain variations. Starting with an overview of the original Barlow Twins framework (Sec. 3.1), we then expound on the integration in our method (Sec. 3.2). We address the challenge of semantically misaligned image pairs through three key strategies: filtering mobile elements in the pooling process, pre-aligning images, and weighting with the confidence estimates, elaborated in Sec. 3.4, Sec. 3.3, and Sec. 3.5, respectively, all contributing to enhanced network robustness in real-world environments.

3.1. Brief introduction to Barlow Twins

The Barlow Twins loss was introduced by Zbontar *et al.* in [30] and originates from the domain of self-supervised learning. In their approach, images from the training dataset

are passed through two randomized augmentation pipelines, to create two varied versions (\mathbf{X}_A and \mathbf{X}_B) of the same original input image. They are then fed into two siamese encoder networks which yields two separate *representations*. Subsequently, these representations are condensed via an average pooling layer and further processed by an attached fully-connected projection network. For a batches of augmented images, this results in two *embedding* vectors, \mathbf{Z}_A and $\mathbf{Z}_B \in M_{b \times p}(\mathbb{R})$ with b being the batch size and p the dimension of the embedding vector. The key idea of [30] is to normalize each dimension of the embedding vectors across its batch dimension and to use the resulting normalized vectors to calculate the cross-correlation matrix $\mathbf{C} \in M_{p \times p}(\mathbb{R})$. Correlation between the vectors is then enforced by the first part of the proposed loss function

$$\mathcal{L}_{\mathcal{BT}} = \sum_i (1 - \mathbf{C}_{ii})^2 + \lambda \sum_i \sum_{j \neq i} \mathbf{C}_{ij}^2 \quad (1)$$

that enforces values of one on the diagonal and thus invariance against the applied augmentations. The second part urges zeros everywhere else, therefore reducing the information redundancy, while $\lambda \in \mathbb{R}$ equilibrates both parts.

The main advantage arises from the absence of a requirement for negative samples, as in contrastive losses.

3.2. Robust semantic segmentation through Barlow Twins

Our network architecture, depicted in Fig. 2, is designed to incorporate the Barlow Twins objective into semantic segmentation networks with the usual encoder(f_θ)-decoder(f_ψ) structure. The fundamental concept is to employ two images captured at the same location but under different conditions (e.g., seasonal changes or weather variations), treating the differences as natural augmentations in the Barlow Twin framework. In this section, we assume that both images are accurately registered and show semantically aligned content, while Secs. 3.4 to 3.5 explain how we deal with non-aligned content.

In the parlance of domain adaptation, we call the image with favorable conditions source image \mathbf{X}_s and the image with less ideal (adverse) conditions target image \mathbf{X}_t . Both images \mathbf{X}_s and \mathbf{X}_t with dimensions (b, c, h, w) traverse the encoder network f_θ , yielding feature maps \mathbf{Y}_s and \mathbf{Y}_t with reduced spatial dimensions (b, c, m, n) , where b is the batch size, c is the channel count, and $m, n < h, w$ being the spatial dimensions, respectively.

These feature maps are then condensed by a pooling operation F into a dimension of $(b, c, 1, 1)$, producing $\bar{\mathbf{Y}}_s$ and $\bar{\mathbf{Y}}_t$. Following the original Barlow Twins protocol (Sec. 3.1), they are fed into a projection network f_ϕ that computes the final embeddings \mathbf{Z}_s and $\mathbf{Z}_t \in M_{b \times \hat{c}}(\mathbb{R})$, with \hat{c} representing the embedding size. The embeddings

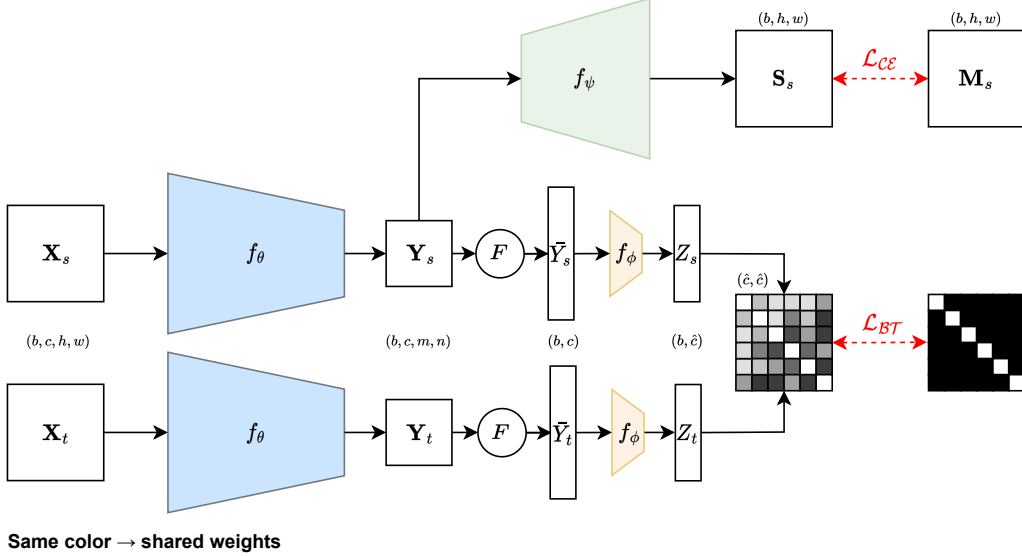


Figure 2. Schematic overview of our proposed semi-supervised semantic segmentation architecture. Images \mathbf{X}_s and \mathbf{X}_t of the same location but with different environmental conditions are processed by the encoder f_θ to obtain feature maps \mathbf{Y}_s and \mathbf{Y}_t . The segmentation head uses \mathbf{Y}_s and the ground truth segmentation mask for the reference condition to generate the final segmentation. The Barlow Twins loss is utilized to enforce robustness against appearance changes caused by adverse weather conditions in \mathbf{X}_t . The feature maps are pooled and passed through a projector network to generate the final embeddings \mathbf{Z}_s and \mathbf{Z}_t . The Barlow Twins loss enforces the embeddings and feature maps to stay close, ensuring robustness against weather changes.

undergo normalization and cross-correlation, forming matrix $\mathbf{C} \in M_{\hat{c} \times \hat{c}}(\mathbb{R})$, establishing the first objective \mathcal{L}_{BT} Eq. (1) to foster domain-robust representations.

The representations from the source path are further processed by the decoder f_ψ (segmentation head), resulting in the creation of a semantic segmentation map, \mathbf{S}_s . This map is scaled to the original input size using bilinear interpolation and evaluated in our second objective using the Cross Entropy loss \mathcal{L}_{CE} .

The combination of both objectives in Eq. (2), guides the network towards assimilating representations resilient to domain variance while maintaining efficiency for semantic segmentation. This fusion of objectives not only facilitates the extraction of latent knowledge but also supports training with weak supervision for domains lacking ground truth data.

$$\mathcal{L} = \mathcal{L}_{CE} + \alpha \mathcal{L}_{BT} \quad (2)$$

It should be highlighted, that our training does not employ annotated images from adverse weather conditions; we rely exclusively on annotated reference images with favorably weather conditions. We argue that this approach proves more advantageous since clear weather reference images are easier to annotate for practical applications and we avoid the additional labeling of adverse image data.

The approach presented so far presumes that the variations in appearance are solely attributable to domain shifts,

rather than dynamic elements or disparate viewpoints. Acknowledging that real-world conditions often present spatial misalignments, especially for datasets depicting the same scene under different weather conditions, the following sections detail our strategies to effectively address and mitigate this challenge.

3.3. Pre-alignment of source and target

To reduce the influence of misalignments between the semantic content in the image pairs caused by slightly different viewpoints, we pre-align the target (adverse condition) to the source (normal condition) image, utilizing the *UAWarpC*-module from [5], pre-trained in a self-supervised manner on MegaDepth [16]. The method returns a warp map aligning the two images, with zero indicating invalid regions (see Fig. 3). The latter is used to find the largest intrinsic rectangle (marked red in Fig. 3) containing the valid warped image region, utilizing the algorithm¹ introduced in [17]. Source, target, and the source segmentation are cropped accordingly.

3.4. Filtering of moving objects

By default, the pooling operation F calculates an single average value for each channel of the whole feature map \mathbf{Y} . While this is already a fairly strong smoothing operation, moving objects, e.g. cars, could disrupt the learning

¹Implementation from <https://github.com/OpenStitching/lir>

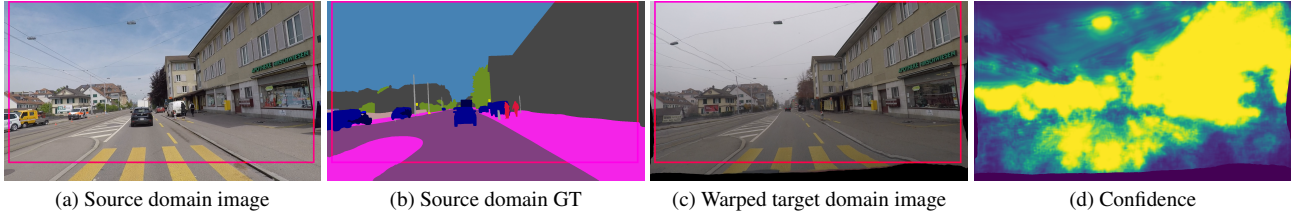


Figure 3. Sample image from the ACDC dataset with the image from the target domain warped to the source domain to align the semantics. The confidence map allows a prediction of the warp quality and is used as described in Sec. 3.5. The red rectangles denote the largest intrinsic rectangles containing only valid image content.

of weather-induced differences in the final embeddings \mathbf{Z} . To this end, we extend the default average pooling F with guidance from the segmentation heads. We generate a binary mask $\mathbf{B} \in M_{b \times m \times n}(\mathbb{R})$ from \mathbf{S} with

$$\mathbf{B}_{i,j} = \begin{cases} 0 & \text{if } i, j \text{ was labeled as a moving object} \\ 1 & \text{otherwise} \end{cases}, \quad (3)$$

to filter areas containing moving objects. Consequently, the average pooling with the exclusion of areas containing moving objects can be formulated as

$$\bar{\mathbf{Y}} = \frac{\sum(\mathbf{Y} \odot \mathbf{B})}{\sum(\mathbf{B}) + \epsilon}, \quad (4)$$

with ϵ being some small constant for numerical stability, $\sum(\cdot)$ the sum over all elements in a matrix and \odot indicating the element-wise product between two matrices.

3.5. Confidence-weighted averaging

The *UAWarpC* module outputs a confidence estimation \mathbf{P}_W , depicted in Fig. 3d, with values within the interval $[0,1]$. This confidence map assigns higher confidence scores to well-matched image regions, such as facades, poles, and trees, and lower scores to areas with less distinctive textures, like the sky or roads. Additionally, moving objects are assigned lower confidence unless, by coincidence, they appear in the same image region. These confidence values are then employed to compute a weighted average for the feature maps \mathbf{Y} .

4. Experiments

In this section, we first describe the datasets (Sec. 4.1) we use for training and evaluation as well as implementation details (Sec. 4.2). We then compare our method against the state of the art for unsupervised domain adaptation (Sec. 4.3) and evaluate the influence of our design choices in Sec. 4.4, the robustness and generalization capabilities in Sec. 4.5, and the influence of the batch size in Sec. 4.6.

4.1. Datasets

A-Cityscapes Halder *et al.* [11] have augmented the well-known Cityscapes dataset [9] to include images depicting rainy and foggy driving conditions. In our experiments, we solely used the provided 2995 training images with a reduced resolution of 1024 by 512 pixels and a simulated rain intensity of 100 mm h^{-1} , as they appeared the most representative of actual conditions. Sample images from this dataset are provided in Fig. 4.



Figure 4. Sample images of the A-Cityscapes dataset with clear and rainy (artificial) weather conditions.

ACDC Sakaridis *et al.* released the ACDC dataset, tailored for semantic segmentation tasks in autonomous driving during adverse weather conditions [23]. For each weather condition (night, rain, fog, snow), 400 training and 100 validation (106 for night) and 500 testing images are available. Every image in the dataset is coupled with a counterpart showing the same scene under clear weather conditions, approximately aligned using GPS data. Originally, the dataset does supply segmentation masks for the adverse conditions, which we employ solely for testing purposes. Therefore, we leveraged a state-of-the-art model – [26], trained on Cityscapes – to generate semantic segmentations for the reference images to generate ground truth labels for the clear condition images.

To optimize training, we refined the dataset by filtering out unsuitable samples, when used in conjunction with our pre-alignment process (see Sec. 3.3). Our exclusion criteria involved two key steps. We first excluded images smaller than 768×768 pixels after cropping to the largest intrinsic rectangle. Next, we conducted a statistical analysis of the confidence maps, focusing on the central 1024×1024

Table 1. Comparison to the state of the art in semi-supervised domain adaptation from Cityscapes \rightarrow ACDC, with the results reported on the official ACDC test set.

Architecture	Method	IoU \uparrow																			
		mean	road	sidewalk	building	wall	fence	pole	traffic light	traffic sign	vegetation	terrain	sky	person	rider	car	truck	bus	train	motorcycle	bicycle
SegFormer	Baseline	59.34	85.71	51.0	76.64	36.36	37.06	45.22	55.65	57.5	77.7	51.95	84.19	60.22	34.69	82.9	61.6	65.45	73.35	37.91	52.43
RefineNet	[24] MGCDA	48.65	73.1	29.01	70.01	19.2	26.44	36.68	52.66	53.24	75.04	31.7	84.75	50.61	25.67	77.7	43.14	45.78	54.98	32.9	41.67
DAFormer	[12] DAFormer	55.36	58.41	51.28	83.98	42.7	35.09	50.69	30.04	56.98	74.84	52.77	51.31	58.25	32.59	82.66	58.27	54.9	82.42	44.07	50.67
DAFormer	[5] Refign	65.51	89.48	63.44	87.3	43.62	34.33	52.28	63.21	61.38	86.94	58.45	95.66	62.14	39.3	84.07	65.7	71.33	85.42	47.94	52.79
SegFormer	[4] CMA	69.12	93.96	75.18	88.56	50.46	45.51	54.85	65.68	64.24	87.08	61.29	95.17	66.99	45.23	86.2	68.64	76.59	83.9	43.32	60.47
DAFormer	[5] Refign-HRDA	72.05	93.82	75.72	90.02	57.93	43.25	55.6	67.42	68.15	88.17	61.79	96.09	67.5	50.75	88.78	75.19	83.44	89.64	54.52	61.2
DeeplabV3	BTSeg-DL (Ours)	56.12	89.78	63.98	82.99	33.34	37.61	50.56	62.45	58.42	81.9	48.94	93.92	53.7	17.46	80.	30.92	32.55	74.71	31.93	40.23
SegFormer	BTSeg (Ours)	70.45	92.92	73.5	88.28	53.6	47.22	56.23	67.9	67.25	86.86	61.5	95.29	67.2	46.8	89.14	73.06	81.61	83.12	49.52	57.47

pixel region to avoid less reliable outer areas. We then computed the proportion of 32×32 patches with an average confidence above 0.6, denoted as p . Observing significant variation in p across different weather conditions, we fitted a gamma distribution to each condition’s histogram. From these distributions, we calculated the mean (μ) and variance (σ^2) and excluded samples where $p < \mu - 3\sigma^2$.

This process resulted in reduced sample counts of 346, 370, 277, and 319 for night, rain, fog, and snow conditions, respectively. The details of the excluded samples are available in the code accompanying our publication.

ACG benchmark Bruggemann *et al.* [4] proposed this benchmark dataset to evaluate the generalization capabilities of models after domain adaptation. The dataset was created through careful selection of images from WildDash2 [31], Foggy Zurich [10, 20], Foggy Driving [21] and BDD100K [29] and contains 121 images with fog, 225 with rain, 276 with snow, and 300 taken during nighttime conditions. In contrast to the ACDC dataset, this dataset includes images with various combined adverse conditions, such as night-time rain, which makes it even more challenging. We exclusively utilize this dataset for testing purposes.

4.2. Implementation details

As proposed by Tsai *et al.* [27], we set λ in Eq. (1) depending on the fraction of on-diagonal ($= n$) and off-diagonal ($= n(n - 1)$) elements following

$$\frac{n}{n(n - 1)} \approx \frac{1}{n} = \lambda, \quad (5)$$

in order to avoid the necessity of tuning it.

In our study, we combined Barlow Twins regularization with two semantic segmentation networks: DeeplabV3 [7] and SegFormer [28]. DeeplabV3 integration is direct due to its shared ResNet-50 encoder with the original Barlow Twins model, which outputs a 2048-dimensional feature

maps \mathbf{Y} . For SegFormer, following Bruggemann *et al.* [4], we resized and concatenated transformer block outputs to match the highest resolution block, resulting in a 1024-dimensional feature maps \mathbf{Y} .

Our projection network comprises two layers with batch normalization (BN) and ReLU activation, reducing input dimensions from 2048 (DeeplabV3) and 1024 (SegFormer) to 512, and then to 256. This contrasts with the original model’s three-layer, 8192-unit projection network, which we found excessively large without added benefit.

We strictly used complete batches during training to accommodate the batch-normalization layer required for the Barlow Twins loss. Both DeeplabV3 and SegFormer were initialized with pretrained weights from ImageNet and Cityscapes datasets, respectively.

Due to the high memory demand of the SegFormer architecture, only one image pair of full-resolution can be fitted into a graphics card with 40 GB of memory. Bruggemann *et al.* [4] accounted for that using gradient accumulation, still using only a batch size of 2. Unfortunately, the BN in the Barlow Twins loss requires higher batch sizes and cannot be employed in combination with gradient accumulation. But it uses BN without learnable parameters, solely for normalization across the batch dimension. Therefore we process the images individually, and store the embeddings \mathbf{Z} in a cache. By setting the cache size to 32, this allows for an effective batch size of 32 for the Barlow Twins loss and also for the overall network, using gradient accumulation.

We trained for 10000 steps on one single GPUs using automatic mixed precision. Data augmentation included random horizontal flipping and cropping to 768x768 (the smallest intrinsic rectangle, as detailed in Sec. 4.1, ACDC paragraph), followed by resizing to 1080x1080 to maintain the original resolution.

In our combined objective function (Eq. (2)), we set α to 0.1 to balance the loss magnitudes. We employed AdamW optimizer with a 0.01 weight decay, a linear warmup for the first 1500 steps, followed by a linear decay. For the first

Table 2. Results of the ablation study performed on the ACDC validation subset reporting the IoU. "BT": usage of the Barlow Twins loss.

Methods				IoU ↑																			
BT	Warp	Crop	Pooling	mean	road	sidewalk	building	wall	fence	pole	traffic light	traffic sign	vegetation	terrain	sky	person	rider	car	truck	bus	train	motorcycle	bicycle
			–	58.32	86.67	51.88	73.01	41.1	36.76	44.41	60.4	57.08	75.73	29.91	96.79	57.4	44.86	74.66	66.62	59.42	59.76	45.37	45.23
x			Average	64.18	90.33	67.43	82.94	47.50	39.14	56.07	74.11	59.40	78.08	39.77	87.63	62.97	37.88	84.32	70.23	79.51	80.73	46.06	35.26
x	x		Average	65.46	91.08	69.50	83.47	49.31	37.53	58.67	73.90	60.31	79.95	42.51	88.76	61.25	42.50	85.22	70.93	86.78	82.63	48.23	31.26
x	x	x	Average	65.71	90.11	66.50	84.25	48.49	39.67	58.16	72.48	61.11	80.16	42.86	89.18	59.48	40.28	85.39	72.57	86.18	84.43	49.34	37.80
x	x	x	Segmentation	65.42	89.74	67.31	83.85	48.88	38.07	59.33	73.19	60.74	80.23	42.83	88.51	59.65	40.34	85.13	75.41	86.07	81.32	48.84	33.50
x	x	x	Confidence	65.23	89.74	66.01	84.02	49.62	39.34	58.70	74.01	61.39	79.78	43.65	88.62	60.66	42.58	84.69	73.46	85.46	72.26	49.43	35.91
x	x	x	Conf. + Seg.	66.20	90.07	67.80	84.17	50.50	39.00	59.92	74.03	61.40	80.32	43.21	88.63	61.04	44.23	84.86	76.50	86.96	83.53	49.02	32.54

2500 steps, we stopped the gradient flow from the projection head to the encoder to avoid noisy updates. We used different learning rates for encoder (1.6×10^{-4}), decoder (1.6×10^{-5}) and the projection network (1.6×10^{-3}).

4.3. Comparison to SOTA in semi-supervised domain adaptation

In Tab. 1, we compare our BTseg method against the state of the art for the domain adaptation from Cityscapes to ACDC. All methods have been evaluated on the official ACDC test set. The first line contains the baseline, a SegFormer [28] network trained solely on Cityscapes in a fully-supervised fashion. Due to the capable Transformer architecture, the baseline already shows good generalization properties, outperforming MGCDA [24] and DAFormer [12] by a great margin. Our implementation, integrated into the DeeplabV3 [7] architecture, also falls behind this strong baseline, while also outperforming DAFormer and MGCDA. In combination with the SegFormer architecture, our method outperforms Refign [5] and CMA [4], while being less complex, as the Barlow Twins loss avoids the necessity of maintaining a list of negative samples, which are needed for the contrastive loss in CMA. Just as reported for CMA, our method also shows a good performance for moving objects. This is remarkable, as these classes are especially challenging to our proposed method, as they violate our assumption of shared content between reference and target image. We suspect that this is due to the rather coarse regularization and the squashing of the (c, m, n) -dimensional feature map to a $(c, 1, 1)$ -dimensional feature vector. The combination of Refign and HRDA [13] slightly outperforms our method; however, it is considerably more complex. In summary, it can be stated that our method performs similarly to the state-of-the-art.

4.4. Ablation study

In this section, we analyze and evaluate our design choices. All numbers are from the ACDC validation set (adverse weather only) and we use the SegFormer configuration de-

scribed in Sec. 4.2 as foundation, but with a randomized cropping to 512 by 512 and without the resizing to 1080 by 1080, facilitating a more efficient training.

Tab. 2 shows the IoU values for the different classes present in the ACDC dataset and the overall mean, respectively. The first row illustrates the results if we train on the labeled source images only and evaluate on the target images. This results in a mean IoU of 58.32% (training SegFormer with the aligned source and target samples and the source segmentation map results in a slightly improved mean IoU of 60.7%). The second row reports the results with our Barlow Twins regularization to enforce the encoder to be robust against the appearance changes caused by the different weather conditions. Subsequently, the mean IoU improves significantly by 5.86 pp. Next, the warping/ alignment between source and target image is added, improving the overall result to 65.5% (third row). The cropping of invalid image regions after the warping process brings another slight improvement. Interestingly, the result slightly decreases when we add segmentation or confidence guided averaging. For the later, this is probably caused by the overly pessimistic confidence estimations in homogeneous image regions, which may impede the training. The segmentation guided averaging is of course susceptible to misclassified image regions, and obstructs the learning of robust encoding, if moving objects by chance align. Finally, the combination of both methods results in our best performing configuration with a mean IoU of 66.2%.

In summary, the results show the intrinsic robustness of the proposed Barlow Twins regularization against slight misalignments, which could be interpreted as natural augmentations additional to the appearance changes caused by the weather conditions.

4.5. Generalization and robustness

The authors of [4] proposed the new composed ACG benchmark to test the robustness and generalization capabilities of networks after the domain adaption from normal to adverse conditions, by exposing them to more diverse and challeng-

Table 3. Comparison against the state of the art on the ACG benchmark ([4]), for the evaluation of robustness and generalization.

Method	mIoU \uparrow				
	fog	night	rain	snow	all
[12]DAFormer	52.6	21.5	47.5	33.6	40.1
[13]HRDA	60.0	27.1	56.2	43.3	48.9
[4]CMA	59.7	40.0	59.6	52.2	51.3
BTSeg (Ours)	61.4	40.2	60.2	50.4	51.8

ing data. Tab. 3 shows the results from recent works, evaluated after the domain adaptation from Cityscapes to ACDC. Our method set a new state of the art on all, but the fog subset, demonstrating its robustness and strong generalization capabilities. It improves significantly over DAFormer and HRDA, which shows the great value of integrating methods from the domain of unsupervised learning, like contrastive learning (CMA [4]) and our method, utilizing the Barlow Twins loss. Though BTSeg improved by a great margin over DAFormer and HRDA, the night subset is still the most challenging. Nevertheless it must be noted, that the night subset is especially challenging, as it also contains images from the other domains but at nighttime (*e.g.* rain at night), which were not present in the ACDC dataset.

We conclude, that our method shows robust performance in the presence of unseen data and even more challenging weather conditions.

4.6. Influence of the Batch Size

The original Barlow Twins paper [30] used a batch size of 2048, but reported also good results for batch sizes as small as 128. This smaller batch size of 128 was also used in [27], where much smaller datasets had been used (Tiny-Imagenet[15] and CIFAR-10[14]). As our datasets are even smaller and the SegFormer architecture needs a lot of memory, we evaluated the performance of our proposed system for batch sizes from 8 to 32. We trained BTSeg with the configuration described in Sec. 4.2, but with an effective batch size for the Barlow Twins loss from 8 to 32. The resulting mean IoU values on the ACDC validation set are shown in Fig. 5. This makes it evident that an effective batch size below 24 impedes the statistics in the BN layer of the Barlow Twins loss, therefore rendering the regularization unstable.

4.7. Robustness to misalignment

To investigate the intrinsic robustness of BTSeg against small misalignments in the semantic content of the image pairs (*e.g.*, due to the imprecise alignment through GPS), we train it in combination with DeeplabV3 on the Cityscapes-A dataset. We trained it with DeeplabV3 on the Cityscapes-A dataset, using original Cityscapes images as references and their rain-augmented versions (100 mm h^{-1}) as tar-

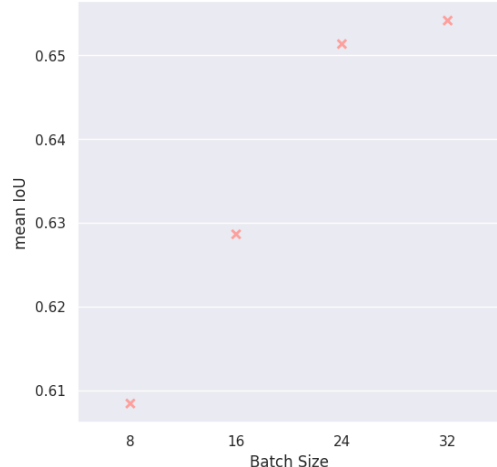


Figure 5. Influence of the batch size hyper parameter on the mean IoU, evaluated on the official ACDC validation set for all conditions.

gets. This setup mirrors ideal conditions for BTSeg, where the source’s segmentation map aligns with the target’s, and rain acts as a randomized augmentation, like originally intended in [30]. Under these conditions, the BTSeg-DeeplabV3 combination achieved a mean IoU of 66.12% on the Cityscapes validation set.

To simulate real-world misalignments, we introduced randomized affine transformations (rotation $[-4^\circ, 4^\circ]$, translation $[-51, 51]$, scale $[0.9, 1.1]$). This resulted in a mean IoU of 63.08%, only marginally lower than the initial result, confirming BTSeg’s robustness to misalignments. We attribute this resilience to the projection network and averaging operation, which collectively focus on general appearance changes due to weather, while still enabling detailed feature map production by the encoder.

5. Conclusion

In this paper, we presented BTSeg, a domain adaptation method for semantically segmenting images captured in challenging weather conditions in a semi-supervised manner. To achieve this goal, we view images of a particular location captured under varying weather conditions as modifications of a shared, unknown base image. By utilizing the Barlow Twins loss, we compel the segmentation network to withstand these assumed augmentations, *i.e.* different weather conditions. Our approach learns from pairs of adverse and clear weather images, requiring a pixel-segmentation mask only for the latter, which is a tremendous advantage as facilitates data collection. Additionally, by utilizing the Barlow Twins loss our method eliminates the necessity for selecting negative samples during the training phase. Not only does our approach keep up with the

strong state of the art for the ACDC dataset and set a new state-of-the-art for the challenging ACG benchmark, it does also present the advantages of streamlined implementation and training, establishing a new standard in efficiency and efficacy.

6. Acknowledgement

This work is supported by the the state of Berlin within the innovation support program ProFIT (IBB) (BerDiBa, grant no. 10185426) and by the German Federal Ministry for Economic Affairs and Climate Action (GEMIMEG-II, grant no. 01MT20001D).

References

- [1] Yuki M. Asano, Christian Rupprecht, and Andrea Vedaldi. Self-labelling via simultaneous clustering and representation learning. In *International Conference on Learning Representations (ICLR)*, 2020. 2
- [2] Adrien Bardes, Jean Ponce, and Yann LeCun. VI-CReg: Variance-Invariance-Covariance Regularization for Self-Supervised Learning. In *International Conference on Learning Representations*, 2022. 2
- [3] Rishika Bhagwatkar, Saurabh Kemekar, Vinay Domatoti, Khursheed Munir Khan, and Anamika Singh. Contrastive Learning-Based Domain Adaptation for Semantic Segmentation. *2022 National Conference on Communications (NCC)*, 00:239–244, 2022. 3
- [4] David Bruggemann, Christos Sakaridis, Tim Brödermann, and Luc Van Gool. Contrastive Model Adaptation for Cross-Condition Robustness in Semantic Segmentation. *arXiv*, 2023. 2, 6, 7, 8
- [5] David Bruggemann, Christos Sakaridis, Prune Truong, and Luc Van Gool. Refign: Align and Refine for Adaptation of Semantic Segmentation to Adverse Conditions. *2023 IEEE/CVF Winter Conference on Applications of Computer Vision (WACV)*, 00:3173–3183, 2023. 2, 4, 6, 7
- [6] Mathilde Caron, Ishan Misra, Julien Mairal, Priya Goyal, Piotr Bojanowski, and Armand Joulin. Unsupervised learning of visual features by contrasting cluster assignments. In *Proceedings of Advances in Neural Information Processing Systems (NeurIPS)*, 2020. 2
- [7] Liang-Chieh Chen, George Papandreou, Florian Schroff, and Hartwig Adam. Rethinking Atrous Convolution for Semantic Image Segmentation. *arXiv*, 2017. 6, 7
- [8] Ting Chen, Simon Kornblith, Mohammad Norouzi, and Geoffrey Hinton. A simple framework for contrastive learning of visual representations. In *International conference on machine learning*, pages 1597–1607. PMLR, 2020. 2
- [9] Marius Cordts, Mohamed Omran, Sebastian Ramos, Timo Rehfeld, Markus Enzweiler, Rodrigo Benenson, Uwe Franke, Stefan Roth, and Bernt Schiele. The Cityscapes Dataset for Semantic Urban Scene Understanding. In *IEEE Conference on Computer Vision and Pattern Recognition (CVPR)*, pages 3213–3223, 2016. 5
- [10] Dengxin Dai, Christos Sakaridis, Simon Hecker, and Luc Van Gool. Curriculum model adaptation with synthetic and real data for semantic foggy scene understanding. *International Journal of Computer Vision*, 128:1182–1204, 2019. 6
- [11] Shirsendu Sukanta Halder, Jean-François Lalonde, and Raoul de Charette. Physics-Based Rendering for Improving Robustness to Rain. *2019 IEEE/CVF International Conference on Computer Vision (ICCV)*, 00:10202–10211, 2019. 5
- [12] Lukas Hoyer, Dengxin Dai, and Luc Van Gool. DAFormer: Improving Network Architectures and Training Strategies for Domain-Adaptive Semantic Segmentation. *2022 IEEE/CVF Conference on Computer Vision and Pattern Recognition (CVPR)*, 00:9914–9925, 2022. 6, 7, 8
- [13] Lukas Hoyer, Dengxin Dai, and Luc Van Gool. HRDA: Context-Aware High-Resolution Domain-Adaptive Semantic Segmentation. In *European Conference on Computer Vision*, pages 372–391. Springer, 2022. 7, 8
- [14] Alex Krizhevsky, Geoffrey Hinton, et al. Learning multiple layers of features from tiny images. 2009. 8
- [15] Ya Le and Xuan Yang. Tiny imagenet visual recognition challenge. *CS 231N*, 7(7):3, 2015. 8
- [16] Zhengqi Li and Noah Snavely. MegaDepth: Learning Single-View Depth Prediction from Internet Photos. *2018 IEEE/CVF Conference on Computer Vision and Pattern Recognition*, pages 2041–2050, 2018. 4
- [17] Zahraa Marzeh, Maryam Tahmasbi, and Narges Mirehi. Algorithm for finding the largest inscribed rectangle in polygon. *Journal of Algorithms and Computation*, 51(1):29–41, 2019. 4
- [18] Ishan Misra and Laurens van der Maaten. Self-supervised learning of pretext-invariant representations. In *CVPR*, 2020. 2
- [19] Narinder Singh Punn and Sonali Agarwal. BT-Unet: A self-supervised learning framework for biomedical image segmentation using barlow twins with U-net models. *Machine Learning*, 111(12):4585–4600, 2022. 3
- [20] Christos Sakaridis, Dengxin Dai, Simon Hecker, and Luc Van Gool. Model adaptation with synthetic and real data for semantic dense foggy scene understanding. In *European Conference on Computer Vision (ECCV)*, pages 707–724, 2018. 6
- [21] Christos Sakaridis, Dengxin Dai, and Luc Van Gool. Semantic foggy scene understanding with synthetic data. *International Journal of Computer Vision*, 126(9):973–992, 2018. 6
- [22] Christos Sakaridis, Dengxin Dai, and Luc Van Gool. Guided Curriculum Model Adaptation and Uncertainty-Aware Evaluation for Semantic Nighttime Image Segmentation. *2019 IEEE/CVF International Conference on Computer Vision (ICCV)*, 00:7373–7382, 2019. 1, 2
- [23] Christos Sakaridis, Dengxin Dai, and Luc Van Gool. Acdc: The adverse conditions dataset with correspondences for semantic driving scene understanding. In *Proceedings of the IEEE/CVF International Conference on Computer Vision*, pages 10765–10775, 2021. 1, 2, 5

- [24] Christos Sakaridis, Dengxin Dai, and Luc Van Gool. Map-Guided Curriculum Domain Adaptation and Uncertainty-Aware Evaluation for Semantic Nighttime Image Segmentation. *IEEE Transactions on Pattern Analysis and Machine Intelligence*, 44(6):3139–3153, 2022. 2, 6, 7
- [25] Rahman Siddiquee, Md Mahfuzur, and Andriy. Redundancy Reduction in Semantic Segmentation of 3D Brain Tumor MRIs. In *Brainlesion: Glioma, Multiple Sclerosis, Stroke and Traumatic Brain Injuries*, pages 163–172. Springer International Publishing, 2022. 3
- [26] Andrew Tao, Karan Sapra, and Bryan Catanzaro. Hierarchical Multi-Scale Attention for Semantic Segmentation. *arXiv*, 2020. 5
- [27] Yao-Hung Hubert Tsai, Shaojie Bai, Louis-Philippe Morency, and Ruslan Salakhutdinov. A Note on Connecting Barlow Twins with Negative-Sample-Free Contrastive Learning. *arXiv*, 2021. 6, 8
- [28] Enze Xie, Wenhai Wang, Zhiding Yu, Anima Anandkumar, Jose M Alvarez, and Ping Luo. SegFormer: Simple and Efficient Design for Semantic Segmentation with Transformers. *Advances in Neural Information Processing Systems*, 34:12077–12090, 2021. 6, 7
- [29] Fisher Yu, Haofeng Chen, Xin Wang, Wenqi Xian, Yingying Chen, Fangchen Liu, Vashisht Madhavan, and Trevor Darrell. Bdd100k: A diverse driving dataset for heterogeneous multitask learning. *2020 IEEE/CVF Conference on Computer Vision and Pattern Recognition (CVPR)*, pages 2633–2642, 2018. 6
- [30] Jure Zbontar, Li Jing, Ishan Misra, Yann LeCun, and Stéphane Deny. Barlow twins: Self-supervised learning via redundancy reduction. In *International Conference on Machine Learning*, pages 12310–12320. PMLR, 2021. 1, 2, 3, 8
- [31] Oliver Zendel, Matthias Schörghuber, Bernhard Rainer, Markus Murschitz, and Csaba Beleznai. Unifying panoptic segmentation for autonomous driving. In *Proceedings of the IEEE/CVF Conference on Computer Vision and Pattern Recognition (CVPR)*, pages 21351–21360, 2022. 6